Experimental Evidence of the Existence of Bound States in the Continuum and Fano Resonances in Solid-Liquid Layered Media

Madiha Amrani,[1] Ilyasse Quotane,[1] Cecile Ghouila-Houri,[2] El Houssaine El Boudouti,[1,*] Leonid Krutyansky,[2,3] Bogdan Piwakowski,[2] Philippe Pernod,[2] Abdelkrim Talbi,[2] and Bahram Djafari-Rouhani[4]

[1] *Laboratoire de Physique de la Matière et du Rayonnement (LPMR), Département de Physique, Faculté des Sciences, Université Mohammed I, Oujda, Morocco*

[2] *Université Lille, CNRS, Centrale Lille, Université Polytechnique Hauts-de-France, UMR 8520 - IEMN, LIA LICS, Lille F-59000, France*

[3] *Prokhorov General Physics Institute of the Russian Academy of Sciences, 38 Vavilov street, Moscow 119991, Russian Federation*

[4] *Institut d'Electronique, de Microélectronique et de Nanotechnologie (IEMN), UMR CNRS 8520, Département de Physique, Université de Lille, Villeneuve d'Ascq 59655, France*

(Received 18 December 2020; revised 21 March 2021; accepted 30 April 2021; published 20 May 2021)

Bound states in continuum (BICs) are resonances with zero width (infinite lifetime) without any leakage into the surrounding media. Their fascinating properties and potential applications have attracted a great deal of interest. In this paper, we give an analytical, numerical, and experimental demonstration of BICs in simple acoustic structures based on either a single solid layer or a triple solid-liquid-solid layer inserted between two liquids. These modes are an intrinsic property of the inserted structure (solid layer or solid-liquid-solid triple layer) with free surfaces and are independent of the surrounding media. Two kinds of BICs are discussed: (i) Fabry-Perot (FP) BICs exist as the consequence of the intersection of the local resonances induced by inserted structure intersect the transmission zeros induced by the solid layers. (ii) Symmetry-protected (SP) BICs occur when appear at normal incidence due to the decoupling of the transverse modes in the solid layer from the longitudinal modes that propagate in the solid and solid-liquid multilayer media. When the incidence angle departs slightly from the BIC conditions, the latter transform into Fano resonances characterized by an asymmetric line shape in the transmission spectra. In addition, we show that the transmission zeros give rise to negative delay times and therefore acoustic superluminal effect. The theoretical results are obtained by means of the Green's function method, whereas the experimental measurements are carried out in ultrasonic domain using plexiglass plates in water. These results may have important applications to realize subsonic and acoustic superluminal phenomena as well as acoustic filters and sensors.

DOI: 10.1103/PhysRevApplied.15.054046

I. INTRODUCTION

In various physical acoustic problems, the scattering objects located in the vicinity of a substrate surface or interface give rise to bound states below the substrate sound lines and resonant states (or leaky waves) above this line. The possibility to realize bound states above the sound line that do not radiate energy into the bulk media is quite intriguing. This kind of modes is known as bound states in continuum (BICs) or trapped modes [1]. They have been interpreted as resonance states with infinite quality factor, whose energies lie in the continuum with zero leakage. In other words, they exhibit the property of remaining confined (as stationary waves) despite their coexistence with continuum states.

Historically, the concept of BICs was proposed as a solution to the Schrödinger equation with a complex artificial potential [2]. Later, the issue of BIC-supporting potentials was addressed again, this time by Herrick and Stillinger [3] who implemented Wigner's idea in a large variety of potentials, and extended it to a two-electron wave function. The concept of BICs is based on the interference phenomena and, hence, can be applied to any other type of waves beyond the quantum systems. Clear experimental observation of BIC was carried out by Plotnik *et al.* in 2011 [4] on photonic crystals. Several theoretical works have demonstrated the possibility to realize BICs in a wide range of physical systems such as photonics [5–15], acoustics [16,17], microwaves [18,19], coaxial and *LC* circuits

*Corresponding author. elboudouti@yahoo.fr

[20,21], and optical waveguide [22]. Their high-quality factors that tend to infinity open the way to many applications such as lasers [12,23], filters [24], acousto-optic modulation [25], and sensors [26–28].

Different mechanisms are behind the occurrence of BICs [1]. Among them, we are more particularly interested in the following two mechanisms that we apply in the acoustic spectrum of solid-fluid multilayer materials. (i) The Fabry-Perot (FP)-type BIC. If radiation loss is the only loss channel for a resonant structure, a FP-type cavity can be created between two resonant structures to trap a radiation wave. The BIC is formed when the quasi-bound states of each resonator interfere with each other through the FP cavity. This is, for example, the case for elastic waves propagating in a system composed of two periodic arrays of cylindrical defects separated by a distance that can support BICs [29]. (ii) Symmetry-protected (SP)-type BIC. If the resonant mode and continuum modes belong to two different symmetry classes, coupling between them will be prohibited. Therefore, the resonance is symmetry-protected from the loss and leakage to the continuum [30,31].

As mentioned previously, BICs appear as resonances with zero width in the transmission spectra as well as in the density of states (DOS). Therefore, they remain confined in some parts of the system even though they coexist with a continuous spectral range of radiating waves that can transport energy away. However, these states can exist only under an appropriate choice of the geometrical or material parameters of the system and/or under specific external excitation conditions [29,32]. Therefore, by slightly detuning the system from the BIC condition (for example, changing an incidence angle), the BIC transforms into a quasi-BIC characterized by a finite width because of its interaction with the surrounding media as well as intrinsic losses. In general, the quasi-BIC manifests itself as a Fano resonance when it falls in the vicinity of a zero of transmission, or as an acoustic-induced transparency (AIT) resonance when it occurs between two close transmission zeros. Let us recall that AIT resonance results from an interference phenomenon where a sharp transparent window (enhanced transmission) associated with steep dispersion is introduced into an opaque medium [33,34], whereas Fano resonance is defined as the result of constructive and destructive interferences of a discrete state with a continuum background [34,35].

In a recent paper [36], we have shown theoretically that simple structures made of a single solid layer or a solid-liquid-solid triple layer immersed in a liquid may support BIC, Fano, and AIT resonances. These resonances are shown through an analysis of the transmission coefficient (amplitude and phase) and DOS obtained using the Green's function method [37,38]. The BICs appear as a consequence of the coincidences at specific incidence angles between transmission zeros induced by the solid layers and discrete modes induced either by the single solid layer or the triple solid-liquid-solid layer with free surface boundary conditions. These modes represent what we called FP BICs. In addition to these modes, there exist also more trivial SP BICs that appear for normal incidence as the result of the decoupling between the transverse modes in the solid layer and the longitudinal modes that propagate in the solid and liquid media. These latter modes have been discussed recently by Mizuno [39] and by us [40]. In this work, we show how a slight deviation of the incidence angle from the normal transforms the BIC to quasi-BICs that manifest themselves under the form of asymmetric Fano resonances.

In this paper, we give experimental evidence of the existence of FP and SP BICs either in a single solid layer or in a solid-liquid-solid layer embedded in a liquid. The solid and liquid media are made of plexiglass and water, respectively, and the experiments are performed through an analysis of the transmission spectra in the ultrasonic domain. These experimental results are confirmed by analytical calculations using the Green's function method where we have introduced appropriately the loss in order to explain the trends of the experimental spectra. In addition, we have performed numerical simulations using a finite-element method based on COMSOL Multiphysics software. Good agreement has been found between theory, simulation, and experimental measurements. In addition to the transmission amplitude, we have also studied the delay time in such structures and shown the possibility of an acoustic superluminal phenomenon induced by the transmission zeros. These experiments represent an experimental demonstration of BICs and Fano resonances in solid-liquid layered media.

The rest of the paper is organized as follows. In Sec. II, we give experimental evidence of the existence of FP and SP BICs in a single solid layer. Section III is devoted to the BICs and Fano resonances in a triple solid-liquid-solid layer. The conclusions are presented in Sec. IV. The details of analytical and numerical calculations as well as the experimental procedure are given the in Supplemental Material [41].

II. SINGLE LAYER

First, we consider the system presented in Fig. 1(a) which is composed of a single solid layer embedded in a liquid with mass density ρ_f and phase velocity v_f. The solid medium is characterized by its thickness d_S, longitudinal speed v_ℓ, transverse speed v_t, and mass density ρ_s. As discussed in more detail in the Supplemental Material SM1 [41], the FP BICs occur at the intersection of the curves representing the eigenmodes of the free solid layer (namely the Lamb modes) as a function of the wavevector parallel to the layers (or, equivalently, the incidence angle), and the similar curves representing the transmission zeros

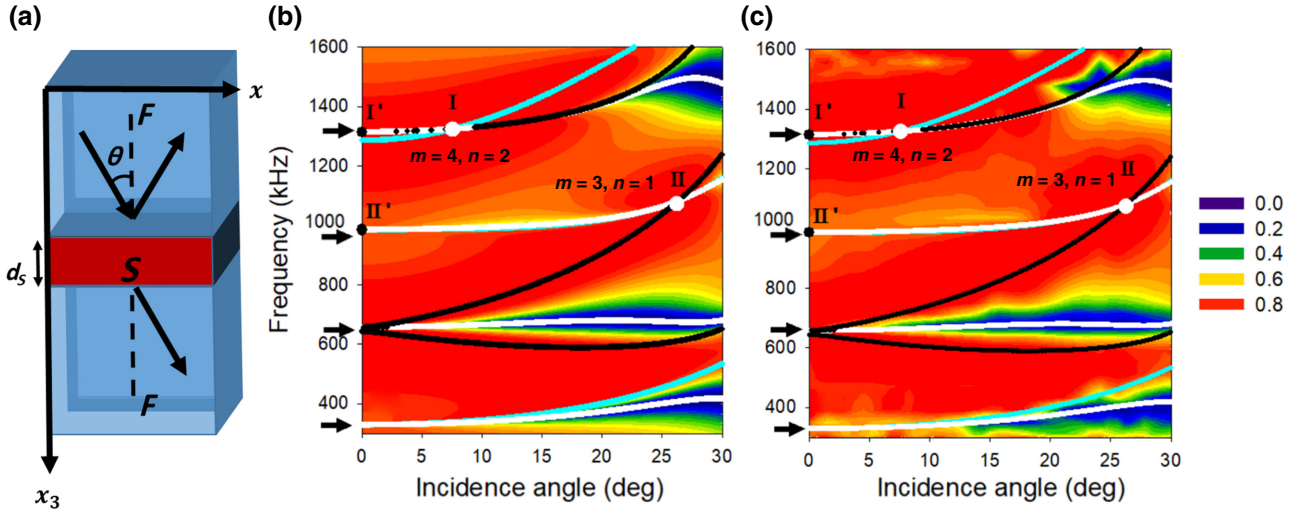

FIG. 1. (a) Schematic representation of a solid layer S (plexiglass) of thickness d_S sandwiched between two semi-infinite liquids F (water). Here θ is the angle of incidence. (b) Theoretical and (c) experimental variation of transmission versus the frequency and the angle of incidence. White dotted curves represent the frequencies of the transmission zeros (total reflection), whereas black and cyan curves are associated with symmetric and antisymmetric modes of the solid layer with free surfaces, respectively. The latter theoretical curves are added on top of the experimental results for the sake of discussion. The black arrows at the normal incidence indicate the positions of the SP BICs.

induced by the immersion of the solid layer in the liquid. Then, the consequences of the BICs and the associated Fano resonances in the transmission coefficient and DOS are discussed. From the analytical analysis of the Lamb modes of the solid layer and the zeros of transmission, one can deduce (see Supplemental Material SM1 [41]) that the frequencies and incidence angles where BICs occur are given by the following:

(i) In the case of oblique incidence ($\theta \neq 0°$), the frequencies and the incidence angles giving the FP BICs are found to be

$$f_{m,n} = \frac{v_l}{\sqrt{(\frac{v_l}{v_t})^2 - 1}} \frac{1}{2d_S} \sqrt{m^2 - n^2} \tag{1}$$

and

$$\sin(\theta) = \frac{v_f}{v_l} \left(\frac{m^2 - n^2 (\frac{v_l}{v_t})^2}{m^2 - n^2} \right)^{1/2}, \tag{2}$$

respectively, where m and n are both odd or both even integers and $m > n$.

Equations (1) and (2) are well known as the coordinates of the crossing points of the uncoupled shear and dilatational modes [42]. These crossing points coincide with the transmission zeros induced by the solid layer giving rise to FP BICs. We have demonstrated that these modes are independent of the nature of the liquids surrounding the solid layer. Let us mention that for the angle (θ) defined by the set of integers (m, n), BICs appear not only at the frequency $f_{m,n}$ but also at all multiples of this frequency ($pf_{m,n}$ where p is a nonzero integer). An interesting point is to know the value of the transmission coefficient t at the limit of the FP BIC where the width of the peak becomes zero. A tedious calculation based on a Taylor expansion of t around $f_{m,n}$ (see Supplemental Material SM1 [41]) leads us to conclude that t reaches a well-defined value, namely a complete transmission $T = 1$ for any combination of the pair of integers $(m, n \neq 0)$ and $T < 1$ for the pair $(m, n = 0)$.

(ii) In the case of normal incidence ($\theta = 0°$), we can show easily from the calculation given in the Supplemental Material SM1 [41] that the SP BICs are the pure transverse modes of a solid layer of thickness d_S with free surface boundary conditions, namely

$$f_p = \frac{p v_t}{2d_S} \tag{3}$$

where p is a nonzero integer. In addition, we show that at SP BICs the transmission coefficient takes a finite value between 0 and 1 (see Supplemental Material SM1, Section A [41]).

For the numerical and experimental results, we consider solid and liquid layers made of plexiglass and water, respectively. The velocities of sound and mass densities are given by $v_t = 1380$ m/s, $v_l = 2700$ m/s and $\rho = 1200$ kg/m^3, respectively, for plexiglass, and $\rho = 1000$ kg/m^3 and $v_l = 1490$ m/s, respectively, for water [36]. It is well known [36] that when a solid layer is embedded between two liquids, the transmission zeros induced

by the solid layer exist only for a range of incident angles such that $0 < \theta < \theta_c$. In the case of plexiglass, $\theta_c = 39°$. It is worth noting that the origin of transmission zeros arise from the destructive interference of longitudinal and transverse waves inside the solid layers, leading to the cancelation of the transmitted waves.

Figures 1(b) and 1(c) give, respectively, the theoretical and experimental variations of the transmission amplitude (with color scale) versus the frequency and the incidence angle for a plexiglass layer of thickness $d_S = 2.1$ mm in water. The experimental results are obtained using two wide-bandwidth acoustic transducers with 1 MHz central frequency, and a network analyzer for scattering parameters S_{ij} measurement (see Supplemental Material SM2 [41] for the experimental setup). The white dots give the curves of transmission zeros as a function of the incidence angle. As mentioned earlier, the transmission zeros are induced by the solid layer embedded between two liquids and are a pure characteristic of the solid. On the other hand, the cyan and black curves show the symmetric and antisymmetric Lamb modes, respectively, of the solid layer with free surfaces. We can see a good agreement between the theoretical and experimental results. The intersection of the transmission zeros curves and Lamb modes curves define the frequencies of the BICs. These modes, involving transverse and longitudinal waves at $\theta \neq 0°$, are known as FP BICs. The first modes are obtained from Eqs. (1) and (2) for ($m = 4$, $n = 2$) and ($m = 3$, $n = 1$), respectively, and are indicated by the white circles marked I and II. The corresponding coordinates are ($\theta_{\rm I} = 7.59°, f_{\rm I} = 1324$ kHz) and ($\theta_{\rm II} = 26.24°, f_{\rm II} = 1072$ kHz), respectively.

In addition to these modes, there exist also the SP BICs marked I′ and II′ corresponding to the pure transverse modes of plexiglass layer, these modes appear for normal incidence ($\theta = 0°$) where the transverse modes do not couple to longitudinal modes in solid and liquid layers. These latter modes are given by Eq. (3) and the corresponding frequencies are 332, 664, 985, 1314,... kHz. These modes are indicated by black arrows in Figs. 1(b) and 1(c). We focus only on the BICs I′ and II′ with $f_{\rm I'} = 1314$ kHz and $f_{\rm II'} = 985$ kHz which are in the range of the experimental observation. Figure 1(c) provides a clear experimental demonstration about the existence of both types of BICs (FP BIC and SP BIC) in a single solid layer immersed in a liquid.

In order to give a better insight about the behavior of the BICs and the associated Fano resonances in the transmission amplitude, we plot in Figs. 2(a)–2(h) the transmission versus the frequency for different values of the incidence angles. The filled circles on the abscissa of Figs. 2(a), 2(c) and 2(g) indicate the positions of the BICs. The green and blue curves correspond to the theoretical results without and with loss, respectively, whereas the red curves give the experimental results. For $\theta = 0°$ [Fig. 2(a)], the transmission coefficient shows ordinary FP oscillations for pure longitudinal waves of a solid layer immersed in water. The pure transverse modes in the single solid layer do not couple to the longitudinal modes. As mentioned earlier, these modes indicated by solid circles on the abscissa axis represent what are called SP BICs. In addition, these modes are hidden and do not give any signature in the transmission spectra, the corresponding resonances have zero width. For θ close to the normal incidence ($\theta = 5.7°$ and $7.1°$) [see Figs. 2(b) and 2(c) respectively], the first BIC (II′) around 1000 kHz gives rise to a quasi-BIC in the transmission spectra, where the transmission zero falls at the vicinity of a Lamb mode. Therefore, the quasi-BICs appear as Fano resonances as shown in Figs. 2(b) and 2(c). These resonances are characterized by an asymmetric line shape (i.e., a resonance close to an antiresonance). Figure 2(d) shows that this resonance remains of Fano shape even far from the incidence angle (i.e., $\theta = 16.7°$). The second BIC labeled (I′) at $\theta = 0°$ and $f_{\rm I'} = 1314$ kHz [Fig. 2(a)], still persists as a quasi-BIC for $\theta \neq 0°$, however, due to the proximity of another FP BIC (I) at $\theta = 7.1°$ around the same frequency, its observation becomes complicated in the transmission spectra. For a large value of the incidence angle ($\theta = 16.7°$), the FP BIC (I) around $f_{\rm I} = 1314$ kHz [Fig. 2(c)] transforms into a quasi-BIC with a Fano shape [Fig. 2(d)]. It is worth noting that the dissipation affects considerably the shape of the Fano resonances, however the main properties of these resonances, namely the presence of a resonance near to an antiresonance, is still visible. In a recent work, Mizuno [39] has given an analytical expression of the transmission coefficient following a Fano form for Fano resonances falling near the normal incidence for an immersed solid layer in a liquid.

In addition to these modes lying near normal incidence, there exists also singular BICs labeled (II) at oblique incidence, falling in the continuum modes of the surrounding liquids without radiating their energy [Fig. 1(b)]. As mentioned previously, this kind of mode is known as a FP BIC. Figures 2(e) and 2(f) clearly show the existence of a dip (quasi-BIC) in the transmission spectra around mode (II) for $\theta < \theta_{\rm II} = 26.5°$. By increasing the incidence angle, the dip collapses for $\theta = \theta_{\rm II}$ [Fig. 2(g)] as a consequence of the existence of both transmission zeros and Lamb modes at exactly the same frequency, giving rise to a zero-width resonance. For $\theta > \theta_{\rm II}$, the dip reappears once again as a Fano resonance at $\theta_{\rm II} = 28.8°$ [Fig. 2(h)]. The experimental results (red curves) are in good agreement with the theoretical results in the presence of loss (blue curves). One should also note that the resonances do not strictly reach zero because of the loss in the solid materials. In the calculation, the loss is introduced by adding a small imaginary part ε to the transverse and longitudinal velocities of sound in the solid layer, namely $v_t(1 + \varepsilon)$ and $v_l(1 + \varepsilon)$, to match the experimental data. It is worth noting that the transmission spectra can be also obtained using COMSOL Multiphysics software considering the actual

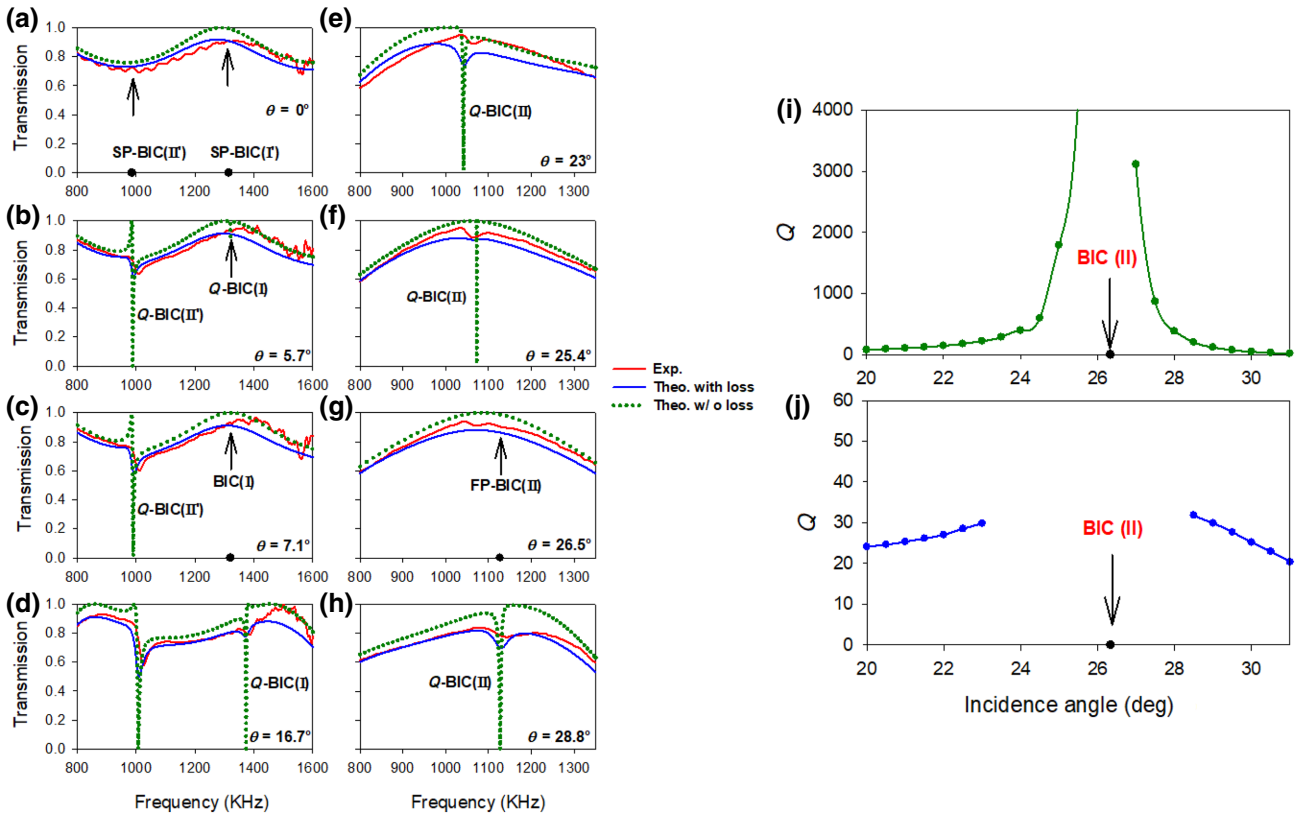

FIG. 2. (a)–(h) Transmission spectra for different values of incidence angles versus the frequency. Green and blue curves correspond to theoretical results without and with loss, respectively, whereas red curves correspond to experimental results. The black arrows indicate the positions of the BICs. (i),(j) Theoretical variation of the quality factor of the transmission resonance around the BIC marked II as function of incidence angle without and with loss, respectively.

scattering geometry in the experiment, an example is provided in the Supplemental Material SM3 [41]. In addition, BIC modes and Fano resonances can be characterized also by the DOS spectra where these modes appear as resonances without and with zero width, respectively. These results are given in the Supplemental Material SM4 [41].

Figures 2(i) and 2(j) represent the quality factor of the transmission around θ_{II} without and with loss, respectively. The quality factor is given by $Q = f_{\mathrm{II}}/\Gamma$ where Γ is the full width at half maximum (FWHM) of the Fano resonance. The latter is obtained from the maximum and minimum of the transmission spectrum around the BIC, which is a characteristic of this type of resonance. In a lossless system [Fig. 2(i)], the quality factor Q increases and it goes to infinity when θ approaches θ_{II}. Indeed, the width Γ of the Fano resonance vanishes at the incidence angle θ_{II}. In a lossy system, one can still define a quality factor, with lower values than in the lossless system, as long as the angle θ is not very close to θ_{II} [see Fig. 2(j)]. However, in the very close vicinity of θ_{II}, the shape of the Fano resonance is affected considerably and it becomes difficult to clearly define its maximum and minimum from which the FWHM and the corresponding quality factor should be deduced. This behavior has been discussed by some of our group in Ref. [43] for BICs in magnonic circuits. In addition, similar results of the quality factor can be obtained from the DOS (see the Supplemental Material SM4 [41]).

III. TRIPLE SOLID-LIQUID-SOLID LAYER

We now consider a more complex geometry of a triple plexiglass-water-plexiglass layer immersed in water [Fig. 3(a)]. In this case, we show that in addition to the BICs and Fano resonances displayed by a single solid layer, there exist other types of BICs and Fano resonances that can be induced by this structure. We demonstrate that, in order to obtain Fano resonances with such structure, the two solid layers should be taken identical, which allows the transmission zeros induced by both solid layers to be obtained at the same frequency [36]. The thickness of all the layers are chosen to be the same $d_{S1} = d_{S2} = d_F = 2.1$ mm. The details of the calculation of dispersion relations, transmission coefficients and DOS for the triple layer, are given in the Supplemental Material SM1 (Section B) [41].

Figures 3(b) and 3(c) give, respectively, the theoretical and experimental variations of the transmission amplitude (with color scale) versus the frequency and the incidence angle. The white dots indicate the frequencies

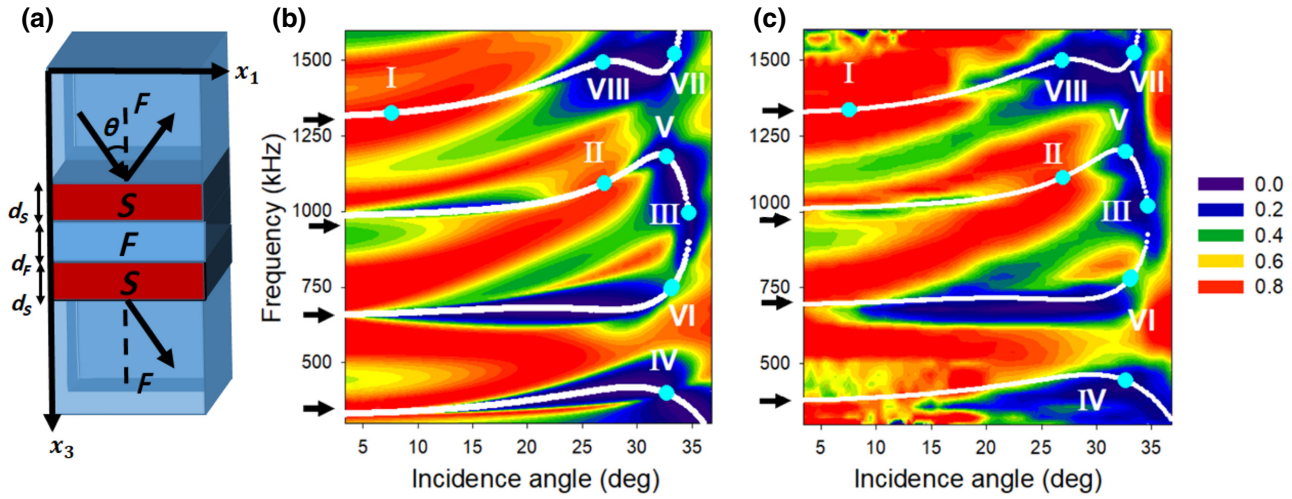

FIG. 3. (a) Schematic representation of a triple layer made of a liquid layer F of thickness d_F sandwiched between two solids S (plexiglass) of thickness d_S. The whole system is inserted between two liquids. (b) Theoretical and (c) experimental variations of transmission (with color scale) versus the frequency and angle of incidence. White dotted curves represent the frequencies of the transmission zeros (total reflection). They are added to the experimental results for the sake of discussion. The black arrows at the normal incidence indicate the positions of the SP BICs.

of the transmission zeros. As mentioned earlier, the transmission zeros induced by the solid layers occur for $\theta < \theta_c \simeq 39°$. It is worth noting here also that the FP BICs appear as the consequence of the intersection of the triple-layer Lamb modes and the transmission zeros. However, we have shown [36] that the FP BICs of a single solid layer still remain in the case of a triple layer. These modes are given by Eqs. (S.26a) and (S.26b) and are represented by the cyan circles marked I, II, VI, and VII. We do not discuss these modes because FP BICs I and II as well as SP BICs indicated by arrows at normal incidence $\theta = 0°$ [Fig. 3(b)] have already been discussed in the case of a single solid layer [Fig. 1(b)]. In addition to these modes, the triple-layer structure induces new additional FP BICs which appear as the intersection between the resonance lines (red area) and the transmission zeros (white dots) marked III, IV, V, and VIII in Fig. 3(b). These modes do not give any signature in the transmission spectra and are characterized by an infinite lifetime. The corresponding coordinates are ($\theta_{\rm III} = 34.7°, f_{\rm III} = 996$ kHz), ($\theta_{\rm IV} = 32.6°, f_{\rm IV} = 398$ kHz), ($\theta_{\rm V} = 32.67°, f_{\rm V} = 1181$ kHz), and ($\theta_{\rm VIII} = 26.9°, f_{\rm VIII} = 1492$ kHz), respectively. These modes are specific modes induced by the triple layer independently of the nature of the surrounding liquids. They are obtained by solving the eigenmodes of the triple layer with free-surface boundary conditions [36] [see Eqs. (S.26a) and (S.26b) in the Supplemental Material SM1, Section B [41]]. One can note also that the experimental results [Fig. 3(c)] are in good agreement with the theoretical results [Fig. 3(b)].

To give a better insight about the behavior of these modes in the transmission spectra, we present in Fig. 4 the transmission through the triple layer around the modes II and IV. Let us start with the mode II at $f = 1050$ kHz for a few incidence angles around this mode. For $\theta = 24.2°$ [Fig. 4(a)], we can see the existence of a dip (quasi-BIC) in the transmission spectra, this dip collapses for $\theta = 26.5°$ [Fig. 4(b)] giving rise to a zero-width resonance. As mentioned before, this kind of mode occurs as the consequence of the coincidence of Lamb modes with the transmission zeros induced by the solid layer. For $\theta > 26.5°$, the resonance reappears once again for $\theta = 28.8°$ [Fig. 4(c)]. Figures 4(d)–4(f) give the transmission spectra around the BIC IV at ($\theta_{\rm IV} = 32.6°$ and $f_{\rm IV} = 398$ kHz). For $\theta = 26.5° < \theta_{\rm IV}$, one can observe the existence of an asymmetric Fano resonance characterized by a transmission zero on only one side. This resonance disappears at $\theta_{\rm IV}$ and $f_{\rm IV}$, giving rise to a FP BIC [Fig. 4(e)]. For $\theta = 34.9° > \theta_{\rm IV}$, the BIC transforms again to a Fano resonance with another shape where the transmission zero precedes the resonance [Fig. 4(f)]. The theoretical and experimental results in Fig. 4 confirm the existence of Fano resonances which collapse, by adjusting the incidence angle, giving rise to a BIC. The experimental results are well fitted by the theoretical results (blue and red curves).

In addition to the transmission amplitude, a complementary quantity that enables to characterize the acoustic wave propagation in solid-liquid layered media is the transmission delay time which is defined as $\tau = (d\Phi/d\omega)$ where Φ is the phase of the transmission and ω is the pulsation. An example of the delay time spectrum for the triple-layer structure is given in Fig. 5(b) together with the transmission amplitude [Fig. 5(a)] for $\theta = 16.58°$. The transmission zeros in Fig. 5(a) around 358, 676, and 1007 kHz give rise to phase jumps of π in the phase of the

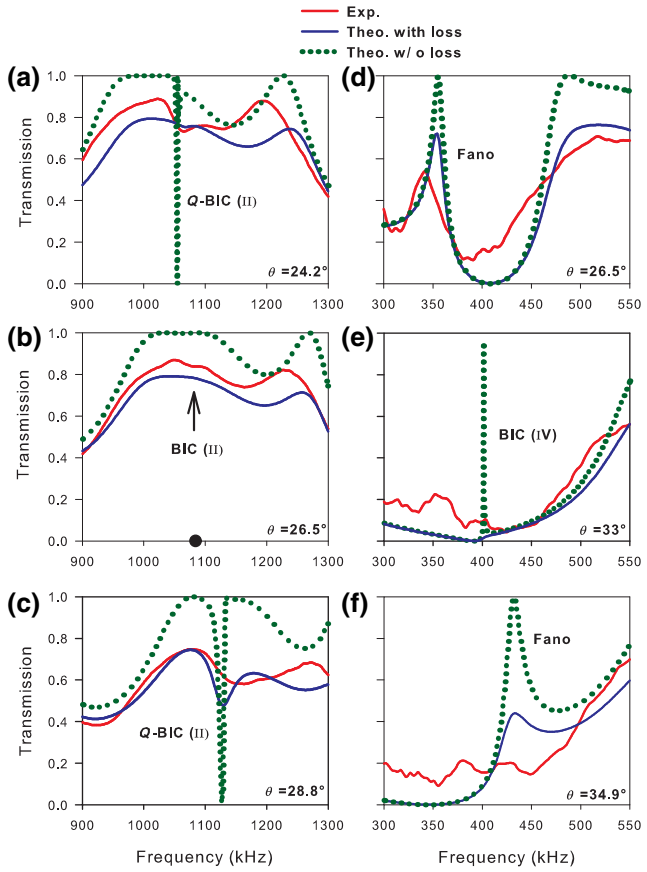

FIG. 4. Transmission spectra through the triple layer versus the frequency for different values of incidence angles. Green and blue curves correspond to theoretical results without and with loss, respectively, whereas red curves correspond to experimental results. The black arrows indicate the positions of the BICs.

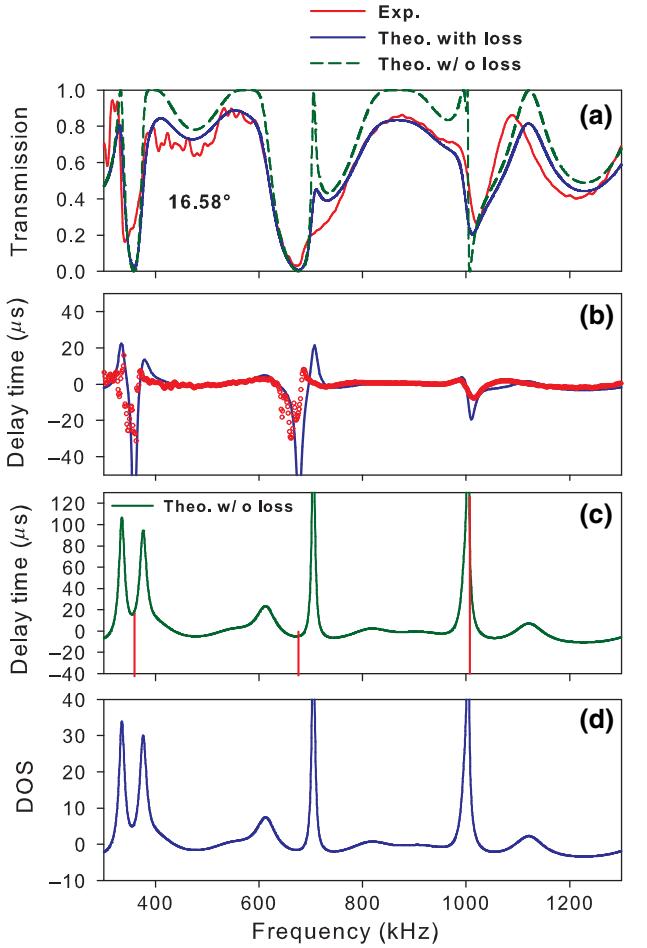

FIG. 5. (a) Amplitude of the transmission versus frequency at the incidence angle $\theta = 16.58°$. The meaning of the curves is the same as in Fig. 4. (b) Delay time versus the frequency. The blue curve corresponds to theoretical results including dissipation, whereas the red curve corresponds to experimental results. (c) Transmission delay time in the absence of loss, the vertical bars indicate the positions of negative delta peaks. (d) Density of states versus the frequency.

transmission and, therefore, negative peaks in the delay time [Fig. 5(b)]. The negative delay time reaches $\tau = -30\ \mu$s in the frequency domain with anomalous dispersion around the transmission zero at 358 kHz, giving rise to a negative group velocity $v_g = L/\tau = -210$ m/s ($L = 6.3$ mm being the length of the triple layer). This behavior is known as a superluminal acoustic phenomenon or pulse tunneling [44,45]. It occurs for evanescent waves when anomalous dispersion is sufficiently strong and the group velocity can exceed the speed of light. However, in optics, it is well established that this phenomenon does not violate the special relativity or causality and the speed of information remains subluminal [46]. In addition, the behavior of the transmission delay time versus the frequency in the absence of loss is plotted in Fig. 5(c) where the negative delay times transform to delta peaks marked by vertical bars. These results show that dissipation is crucial to broaden the negative delta peaks which enables an experimental measurement of the negative group velocity. The different modes of the system appear as resonant peaks in the DOS as described in Fig. 5(d). One should note that, except for the negative delta peaks, the DOS is exactly proportional to the lossless delay time [Fig. 5(c)] [47]. The behavior of the Fano resonance around 700 kHz and its transformation to a BIC in the delay time is discussed in the Supplemental Material SM5 [41]. The analysis and exploitation of the delay times are useful for the characterization of the resonances and BICs, as reported here. The correspondences between DOS and delay times are similar to those reported recently by some of our group in photonic coaxial cables [48].

IV. CONCLUSION

In summary, we have given a clear experimental evidence about the existence of BICs and Fano resonances in simple structures made of single plexiglass layer or a

plexiglass-water-plexiglass triple layer immersed in water in the ultrasonic domain. The experimental measurements are confirmed by analytical calculations obtained with the help of the Green's function method as well as simulation results obtained using a finite-element method. We demonstrate the existence of two types of BICs, namely FP and SP BICs. FP BICs exist as a consequence of the intersection of symmetric and/or antisymmetric Lamb modes and transmission zeros of the solid layer, whereas SP BICs occur as a consequence of the decoupling between longitudinal and transverse waves in the solid layer at normal incidence. These modes appear as resonances with zero width in the transmission spectra, as well as in the DOS. By slightly detuning the incidence angle from that corresponding to BICs, one can obtain Fano resonances. These resonances, characterized by an asymmetric line shape, lie in the vicinity of a transmission zero. A study of the delay time enables us to deduce complementary information on the wave propagation, such as the superluminal acoustic phenomenon associated with negative delay times around the transmission zeros induced by solid layers. We present experimental evidence showing the existence of BICs and Fano resonances in simple solid-liquid layered acoustic structures. These features are very sensitive to small perturbations and therefore can find useful applications as efficient fluid sensors [49]. Another perspective of our work is the possibility of realizing AIT resonances if the thicknesses of the two solids in the triple-layer structure are chosen to be slightly different from each other and produce two close but distinct zeros of transmission. An AIT resonance can be achieved between these zeros at an appropriate incidence angle by adjusting the thickness of the fluid separating the solid layers. Although the experiments presented in this paper are performed by using plexiglass layers, other solids with less dissipation such as Si and SiO_2 and showing highest-quality Fano resonances would be worthy of investigation. The BICs discussed in this work can be applied to realize liquid-sensitive sensors with high-quality factors. Indeed, adding a concentration of albumin to water can shift and broaden the BIC of pure water by transforming it into a Fano resonance for different concentrations of albumin. The frequency shift of the resonance is very sensitive to the variation of the concentration of albumin. Finally, similar theoretical and experimental works can be applied to periodic solid-liquid structures where the BICs can fall inside the allowed bands of the phononic crystal. The works cited are now in progress.

[1] C. W. Hsu, Bo Zhen, A. D. Stone, J. D. Joannopoulos, and M. Soljačcić, Bound states in the continuum, Nat. Rev. Mater. **1**, 16048 (2016).

[2] J. Von Neumann and E. P. Wigner, Uber merkwiirdige diskrete eigenwerte, Phys. Z. **30**, 465 (1929).

[3] F. H. Stillinger and D. R. Herrick, Bound states in the continuum, Phys. Rev. A **11**, 446 (1975).

[4] Y. Plotnik, O. Peleg, F. Dreisow, M. Heinrich, S. Nolte, A. Szameit, and M. Segev, Experimental Observation of Optical Bound States in the Continuum, Phys. Rev. Lett. **107**, 183901 (2011).

[5] D. C. Marinica, A. G. Borisov, and S. V. Shabanov, Bound States in the Continuum in Photonics, Phys. Rev. Lett. **100**, 183902 (2008).

[6] A. Taghizadeh and I. S. Chung, Quasi bound states in the continuum with few unit cells of photonic crystal slab, Appl. Phys. Lett. **111**, 031114 (2017).

[7] E. N. Bulgakov and A. F. Sadreev, Bound states in the continuum in photonic waveguides inspired by defects, Phys. Rev. B **78**, 075105 (2008).

[8] F. Monticone and A. Alu, Embedded Photonic Eigenvalues in 3D Nanostructures, Phys. Rev. Lett. **112**, 213903 (2014).

[9] A. Cerjan, C. W. Hsu, and M. C. Rechtsman, Bound States in the Continuum through Environmental Design, Phys. Rev. Lett. **123**, 023902 (2019).

[10] E. N. Bulgakov and A. F. Sadreev, Robust bound state in the continuum in a nonlinear microcavity embedded in a photonic crystal waveguide, Opt. Lett. **39**, 5212 (2014).

[11] N. Rivera, C. W. Hsu, B. Zhen, H. Buljan, J. D. Joannopoulos, and M. Soljačić, Controlling directionality and dimensionality of radiation by perturbing separable bound states in the continuum, Sci. Rep. **6**, 33394 (2016).

[12] A. Kodigala, T. Lepetit, Q. Gu, B. Bahari, Y. Fainman, and B. Kantè, Lasing action from photonic bound states in continuum, Nature. **541**, 196 (2017).

[13] H. M. Doeleman, F. Monticone, W. den Hollander, A. Alù, and A. F. Koenderink, Experimental observation of a polarization vortex at an optical bound state in the continuum, Nat. Photonics **12**, 397 (2018).

[14] J. Gomis-Bresco, D. Artigas, and L. Torner, Anisotropy-induced photonic bound states in the continuum, Nat. Photonics **11**, 232 (2017).

[15] P. S. Pankin, B. R. Wu, J. H. Yang, K.-P. Chen, I. V. Timofeev, and A. F. Sadreev, One-dimensional photonic bound states in the continuum, Communic. Phys. **3**, 91 (2020).

[16] S. Hein, W. Koch, and L. Nannen, Trapped modes and Fano resonances in two-dimensional acoustical duct-cavity systems, J. Fluid Mech. **692**, 257 (2012).

[17] A. A. Lyapina, D. N. Maksimov, A. S. Pilipchuk, and A. F. Sadreev, Bound states in the continuum in open acoustic resonators, J. Fluid Mech. **780**, 370 (2015).

[18] T. Lepetit, E. Akmansoy, J-P. Ganne, and J.-M. Lourtioz, Resonance continuum coupling in high-permittivity dielectric metamaterials, Phys. Rev. B **82**, 195307 (2010).

[19] T. Lepetit and B. Kanté, Controlling multipolar radiation with symmetries for electromagnetic bound states in the continuum, Phys. Rev. B **90**, 241103 (2014).

[20] A. Mouadili, E. H. El Boudouti, A. Soltani, A. Talbi, A. Akjouj, and B. Djafari-Rouhani, Theoretical and experimental evidence of Fano-like resonances in simple monomode photonic circuits, J. Appl. Phys. **113**, 164101 (2013).

[21] Z. Li, J. Wu, X. Huang, J. Lu, F. Li, W. Deng, and Z. Liu, Bound state in the continuum in topological inductor capacitor circuit, Appl. Phys. Lett. **116**, 263501 (2020).

[22] E. A. Bezus, D. A. Bykov, and L. L. Doskolovich, Bound states in the continuum and high-Q resonances supported by a dielectric ridge on a slab waveguide, Photonics Res. **6**, 1084 (2018).

[23] K. Hirose, Y. Liang, Y. Kurosaka, A. Watanabe, T. Sugiyama, and S. Noda, Watt-class high-power, high-beam-quality photonic-crystal lasers, Nat. Photonics **406**, 411 (2014).

[24] X. Cui, H. Tian, Y. Du, G. Shi, and Z. Zhou, Normal incidence filters using symmetry-protected modes in dielectric subwavelength gratings, Sci. Rep. **6**, 36066 (2016).

[25] Z. Yu and X. Sun, Acousto-optic modulation of photonic bound state in the continuum, Light Sci. Appl. **9**, 1 (2020).

[26] A. A. Yanik, A. E. Cetin, M. Huang, A. Artar, S. H. Mousavi, A. Khanikaev, J. H. Connor, G. Shvets, and H. Altug, Seeing protein monolayers with naked eye through plasmonic Fano resonances, Proc. Natl Acad. Sci. **108**, 11784 (2011).

[27] B. Zeng, Y. Gao, and F. J. Bartoli, Rapid and highly sensitive detection using Fano resonances in ultrathin plasmonic nanogratings, Appl. Phys. Lett. **105**, 161106 (2014).

[28] S. Romano, G. Zito, S. Torino, G. Calafiore, E. Penzo, G. Coppola, S. Cabrini, I. Rendina, and V. Mocella, Dielectric nanohole array metasurface for high-resolution near-field sensing and imaging, Photonics Res. **6**, 726 (2018).

[29] O. Haq and S. V. Shabanov, Bound states in the continuum in elasticity, Wave Motion **103**, 102718 (2021).

[30] Z. F. Sadrieva, M. A. Belyakov, M. A. Balezin, P. V. Kapitanova, E. A. Nenasheva, A. F. Sadreev, and A. A. Bogdanov, Experimental observation of a symmetry-protected bound state in the continuum in a chain of dielectric disks, Phys. Rev. A **99**, 053804 (2019).

[31] L. Cong and R. Singh, Symmetry-protected dual bound states in the continuum in metamaterials, Adv. Optical Mater. **7**, 1900383 (2019).

[32] T. Mrabti, Z. Labdouti, A. Mouadili, E. H. El Boudouti, and B. Djafari-Rouhani, Aharonov-bohm-effect induced transparency and reflection in mesoscopic rings side coupled to a quantum wire, Physica E **116**, 113770 (2020).

[33] S. E. Harris, Electromagnetically induced transparency, Phys. Today **50**, 36 (1997).

[34] A. E. Miroshnichenko, S. Flach, and Y. S. Kivshar, Fano resonances in nanoscale structures, Rev. Mod. Phys. **82**, 2257 (2010).

[35] U. Fano, Effects of configuration interaction on intensities and phase shifts, Phys. Rev. **124**, 1866 (1961).

[36] I. Quotane, E. H. El Boudouti, and B. Djafari-Rouhani, Trapped-mode-induced Fano resonance and acoustical transparency in a one-dimensional solid-fluid phononic crystal, Phys. Rev. B **97**, 024304 (2018).

[37] E. H. El Boudouti, B. Djafari-Rouhani, A. Akjouj, and L. Dobrzynski, Acoustic waves in solid and fluid layered materials, Surf. Sci. Rep. **64**, 471 (2009).

[38] L. Dobrzynski, E. H. El Boudouti, A. Akjouj, Y. Pennec, H. Al-Wahsh, G. Lévêque, and B. Djafari-Rouhani, *Phononics* (Elsevier, Amsterdam, 2017).

[39] S. Mizuno, Fano resonances and bound states in the continuum in a simple phononic system, Appl. Phys. Express **12**, 035504 (2019).

[40] M. Amrani, I. Quotane, C. Ghouila-Houri, E. H. El Boudouti, B. Djafari Rouhani, L. Krutyanskiy, B. Piwakowski, and A. Talbi, Two types of bound in continuum states in a solid layer embedded in a liquid, Proceedings of Meetings on Acoustics **38**, 045034 (2020).

[41] See the Supplemental Material at http://link.aps.org/supplemental/10.1103/PhysRevApplied.15.054046 for the details of analytical calculation based on the Green's function method (SM1), the experimental procedure (SM2), the numerical calculation using Comsol software (SM3), the DOS calculation (SM4), and the behavior of BIC and Fano resonance in the delay time (SM5).

[42] I. A. Veres, T. Berer, C. Grünsteidl, and P. Burgholzer, On the crossing points of the lamb modes and the maxima and minima of displacements observed at the surface, Ultrasonics **54**, 759 (2014).

[43] A. Mouadili, E. H. El Boudouti, A. Akjouj, H. Al-Wahsh, B. Djafari-Rouhani, and L. Dobrzynski, Effect of damping on magnetic induced resonances in cross waveguide structures, J. Supercond. Nov. Magn. **34**, 597 (2021).

[44] W. M. Robertson, J. Pappafotis, P. Flannigan, J. Cathey, B. Cathey, and C. Klaus, Sound beyond the speed of light: Measurement of negative group velocity in an acoustic loop filter, Appl. Phys. Lett. **90**, 014102 (2007).

[45] X. J. Li, C. Xue, L. Fan, S. Y. Zhang, Z. Chen, J. Ding, and H. Zhang, Simultaneous realization of negative group velocity, fast and slow acoustic waves in a metamateria, Appl. Phys. Lett. **108**, 231904 (2016).

[46] G. Nimtz, Superluminal speed of information, Nature (London) **429**, 6987 (2004).

[47] Y. El Hassouani, E. H. El Boudouti, B. Djafari-Rouhani, and H. Aynaou, Sagittal acoustic waves in finite solid-fluid superlattices: Band-gap structure, surface and confined modes, and omnidirectional reflection and selective transmission, Phys. Rev. B **78**, 174306 (2008).

[48] S. Khattou, M. Amrani, A. Mouadili, E. H. El Boudouti, A. Talbi, A. Akjouj, and Bahram Djafari-Rouhani, Comparison of density of states and scattering parameters in coaxial photonic crystals: Theory and experiment, Phys. Rev. B **102**, 165310 (2020).

[49] S. E. Zaki, A. Mehaney, H. M. Hassanein, and A. H. Aly, Fano resonance based defected 1D phononic crystal for highly sensitive gas sensing applications, Sci. Rep. **10**, 17979 (2020).